Journal of Hazardous Materials 187 (2011) 264–273

Contents lists available at ScienceDirect

Journal of Hazardous Materials

journal homepage: www.elsevier.com/locate/jhazmat

$MnCl_2$ and $MgCl_2$ for the removal of reactive dye Levafix Brilliant Blue EBRA from synthetic textile wastewaters: An adsorption/aggregation mechanism

A.Z. Bouyakoub[a,b,*], B.S. Lartiges[a,c,*], R. Ouhib[b], S. Kacha[b], A.G. El Samrani[d], J. Ghanbaja[e], O. Barres[a]

[a] Nancy University - LEM-ENSG/INPL-CNRS, Pôle de l'Eau, 15 Avenue du Charmois, BP 40 54501 Vandoeuvre Cedex, France
[b] University of DjillaliLiabes - LMSR, BP 89, 22000 Sidi Bel Abbes, Algeria
[c] University of Toulouse (UPS) – Geosciences Environment Toulouse UMR 5563, 14 Av. E. Belin, F-31400 Toulouse, France
[d] Lebanese University – Graduate School of Sciences & Technologies, Campus Rafic Hariri-Hadath Beyrouth, Lebanon
[e] Nancy University - SCMEM-FST/UHP, 7137 boulevard des Aiguillettes, BP 239 54506 Vandoeuvre Cedex, France

ARTICLE INFO

Article history:
Received 29 July 2010
Received in revised form
27 December 2010
Accepted 5 January 2011
Available online 12 January 2011

Keywords:
Azo-dye pigment
Levafix Brilliant Blue EBRA
$MgCl_2$
$MnCl_2$
Brucite
Feitknechite

ABSTRACT

Two divalent cation-based coagulants, magnesium chloride and manganese chloride, were used to treat synthetic textile wastewaters containing the azo-dye pigment Levafix Brilliant Blue EBRA. The jar-tests were performed in the presence or absence of auxiliary dyeing chemicals. They proved that (i) both divalent cation-based coagulants were effective in the treatment of those alkaline effluents, (ii) better performances in terms of color removal, residual turbidity, and settled volume, were achieved with manganese chloride, and (iii) the presence of dyeing auxiliaries significantly increases the required coagulant demand for treating the textile effluent. The dye removal mechanisms were investigated by combining observations of freeze-dried sediments with transmission electron microscopy coupled with energy-dispersive X-ray spectroscopy and selected area electron diffraction, Fourier transform infrared spectroscopy, adsorption experiments, and aggregates size measurements with a laser sizer under cyclic shear conditions. The results show that brucite ($Mg(OH)_2$) particles are formed when applying $MgCl_2$ to the textile wastewaters, whereas a mixture of feitknechite (β-MnOOH) and hausmannite (Mn_3O_4) is obtained when using $MnCl_2$. More poorly crystallized particles are formed in presence of auxiliary dyeing chemicals. The adsorption experiments suggested that the azo-dye pigment adsorbs onto the surface of precipitating phases, whereas the aggregation dynamics indicated that a charge-neutralization mechanism underlies the formation of aggregates. The dye removal is then consistent with a precipitation/adsorption mechanism.

1. Introduction

Textile dyeing is one of the main contributing categories to the ecological footprint of textile production [1]. Besides a high water consumption, this process generates colored wastewaters that are particularly difficult to treat. Indeed, textile effluents are characterized by a large amount of dyestuffs, a strong alkalinity, a high chemical oxygen demand, and a low biodegradability [2]. In addition, the chemical structure of dyes contained in the effluents resists degradation in most conventional wastewater treatment processes because of their stability to oxidizing agents and to microorganisms [3–5]. As most dyes have been shown to be toxic to some organisms and to cause direct destruction of aquatic communities [6], the discharge of partially treated effluents often severely impacts the receiving water systems [7].

Various methods have been proposed for the treatment of colored wastewaters, namely, oxidation [8–10], electrolysis [11–13], biodegradation [14,15], adsorption [6,16–18], chemical coagulation [5,6,19–25] and membrane filtration [1,5,26–28]. The oxidation processes certainly represent the best techniques to eliminate the total organic carbon, but they have been shown to be effective only at very low dye concentrations [5,25]. Electrochemical processes can be easily adapted to the polluant load but the formation of an abundant hydroxide sludge represents a major drawback [24]. Conventional biological process is generally shown to be less efficient at degrading dye pigments because of their complicated aromatic structure and molecular size [25]. Both coagulation and adsorption processes have been proven to be highly effective for decoloring textile effluent, but the costs associated with actived carbon requirement and sludge treatment appear prohibitive [24,25]. Finally, the performance of membrane processes for the removal of reactive dyes is often limited by severe fouling [24].

* Corresponding authors at: University of Toulouse (UPS) - Geosciences Environment Toulouse UMR 5563, 14 Av. E. Belin, F-31400 Toulouse.
E-mail addresses: zbouyakoub@yahoo.fr (A.Z. Bouyakoub), bruno.lartiges@lmtg.obs-mip.fr (B.S. Lartiges).

0304-3894/$ – see front matter © 2011 Elsevier B.V. All rights reserved.
doi:10.1016/j.jhazmat.2011.01.008

Table 1
Nature of dyeing auxiliary chemicals.

Product	Chemical nature	Use
Migrasol MV	Amide acrylic polymer/sodium acrylate	Anti-migrating agent
Meropan XR Pearls	Mononitrobenzene sulphonate of sodium	Oxidizing agent
Subitol RNC	Special sulfonates	Dampening agent
Urea	Diamide carbonic acid	Stabilizing agent

Chemical coagulation using magnesium salts has been shown to be an effective alternative to conventional treatments of textile effluents, especially since (i) conventional coagulants such as alum or PAC are not operational at pHs encountered in typical textile wastewaters [41] and (ii) magnesium can be easily recovered from the sludge and reused [25]. However, the mechanisms by which the dye pigments are amenable to removal in such a treatment have only been roughly examined [21,23,29,30]. In particular, the adsorptive-coagulating mechanism initially suggested by Leentvaar and Rebhun [30], needs to be further substantiated. The purpose of this work is then to provide some new insights into the ability of two divalent cation-based coagulants, $MgCl_2$ and $MnCl_2$, to eliminate the reactive dye Levafix Brilliant Blue EBRA from synthetic textile wastewaters. Levafix Brilliant Blue EBRA is a pigment dye mainly used for jeans dyeing. Although this compound is abundantly present in textile effluents, only scarce data are available regarding its removal from wastewaters [23]. Furthermore, the influence of auxiliary dyeing chemicals on the process of dye removal is commonly overlooked in the literature. Therefore, we used two types of synthetic effluents, i.e. EBRA reactive dye in the presence or absence of dyeing auxiliaries, to investigate the importance of those chemicals on dye coagulation. The elimination of pigment dye was assessed by jar-test coupled with UV–vis spectroscopy measurements, the mineral species generated by the chemical treatment were identified using Fourier transform infrared spectroscopy and transmission electron microscopy combined with energy-dispersive X-ray spectroscopy (TEM–EDXS), and the structural characteristics of aggregates were examined with a laser sizer under cyclic shear conditions.

2. Experimental

2.1. Chemicals

The commercial dye used in this study, Levafix Brillant Blue (EBRA), was kindly supplied by DENIM, a jeans textile manufacturer from Algeria. The patent protecting its chemical formula (Patent no. F 51942), states that the chromophore part can be either dichloroquinoxaline, monofluorotriazine, or difluorochloropyridine. Dyeing auxiliary chemicals, Migrasol MV, Meropan XR, and Subitol RNC, were graciously provided by CHTR (France). Urea (99%) and $NaHCO_3$ (99.7%) were acquired from Acros organics and Aldrich, respectively. The chemical nature of these products and their role upon dyeing, are indicated in Table 1. Unlike EBRA dye which fixation rate on the textile fiber is about 70%, the dyeing auxiliary chemicals end up in the effluent.

Reagent grade $MnCl_2{\cdot}4H_2O$ (99%) and $MgCl_2{\cdot}6H_2O$ (99%) obtained from Acros organics and Sigma, respectively, were used as coagulants. They were both freshly prepared as 1 M coagulant stock solutions with deionized water (MilliQ-plus 18.2 MΩ).

2.2. Preparation of synthetic waters

Two types of synthetic effluents were used in this study. SW1 was prepared by dissolving EBRA reactive dye (30 mg/l) and $NaHCO_3$ (1 g/l) in deionized water. SW2 was prepared by adding to SW1 the various dyeing auxiliary chemicals, i.e. urea (50 g/l), Subitol RNC (5 g/l), Rapidoprint XR (3 g/l), and Migrasol MV (10 g/l). Prior to coagulation treatment, the synthetic waters were first heated at 50–70 °C for 15 min to provide hydrolysis conditions similar to those encountered during dyeing. They were then left to cool down to room temperature (25 °C). The EBRA concentration in synthetic effluents was determined from the initial dye concentration used by DENIM in industrial operation (100 mg/l) and from the dye fixation rate (70%).

2.3. Aggregation procedure and supernatant characterization

In order to limit the consumption of reagents, coagulation studies were conducted in 150 ml reactors (60 mm diameter and 80 mm high) fitted with 4 Plexiglas baffles (8 mm × 70 mm). Stirring was carried out with a 3.15 cm × 1.5 cm blade positioned at one-third the height of the reactor from the bottom. The pH of synthetic waters was adjusted to 12, pH of DENIM textile effluents, by dropwise addition of NaOH 1 N. The coagulant was then added under agitation using a micro-pipette (Eppendorf) at a point just below the free surface of the effluent. Mixing followed a conventional jar test procedure with rapid mixing at 250 rpm for 3 min and slow stirring at 60 rpm for 20 min. The pH was not readjusted after coagulant addition.

At the end of mixing, the coagulated suspension was allowed to settle in graduated Imhoff cones for 2 h. The sediment volume was measured and 20 ml of supernatant was siphoned with a syringe for residual turbidity assessment (Hach 2100N turbidimeter). The collected supernatant was then filtered through a 0.22 μm pore size cellulose-acetate filter (Macherey-Nagel) for pH (LPH330T pH-meter), conductivity (CD 810 Tacussel), and color measurements. EBRA absorbance was measured at $\lambda = 590$ nm using a Shimadzu UV-2501 spectrophotometer. The percentage of color removal was calculated by comparing the absorbance values of original synthetic effluent and supernatant. Ultrapure water served as reference.

2.4. Aggregate size measurements

In addition to classical jar-tests, the coagulation dynamics was investigated by monitoring the floc size distribution obtained at optimal coagulant concentration under cyclic step changes in agitation. The floc size distribution was measured on-line with a Malvern Mastersizer using a particle size detection range of 1.2–600 μm. An experimental set-up similar to that described in Chaignon et al. [31] was used in this study. To avoid multiple scattering in the measurement cell, the coagulated suspensions were diluted with synthetic water prepared without EBRA dye and were adjusted to the pH of the corresponding suspension. The dilution was adjusted to yield a 5% volume concentration for all coagulated suspensions. Size measurements were averaged over 1 s and taken every 2 s. The floc size distributions are monomodal, and can be represented by their mean floc diameter d_m. The fractal structure of aggregates was determined from the equation $\phi \sim {d_m}^{(3-D_f)}$, where ϕ is the volume fraction given by the particle sizer, and D_f is the mass fractal dimension of aggregates [31].

2.5. Sediment characterization

The nature of aggregates obtained at optimal coagulant concentration was examined by (i) TEM–EDXS on centrifuged (Eppendorf 5804–2860 g for 10 min) and then freeze-dried sediment (EL 105 Sentry) and (ii) FTIR on dialyzed (Spectro Por 6 – MWCO 2000) and then freeze-dried sediment. Dialysis was required to remove excess salt originating from dyeing auxiliary chemicals. Electron microscopy observations were performed with with a Philips CM20 TEM (200 kV) coupled with an Princeton Gamma Tech energy dis-

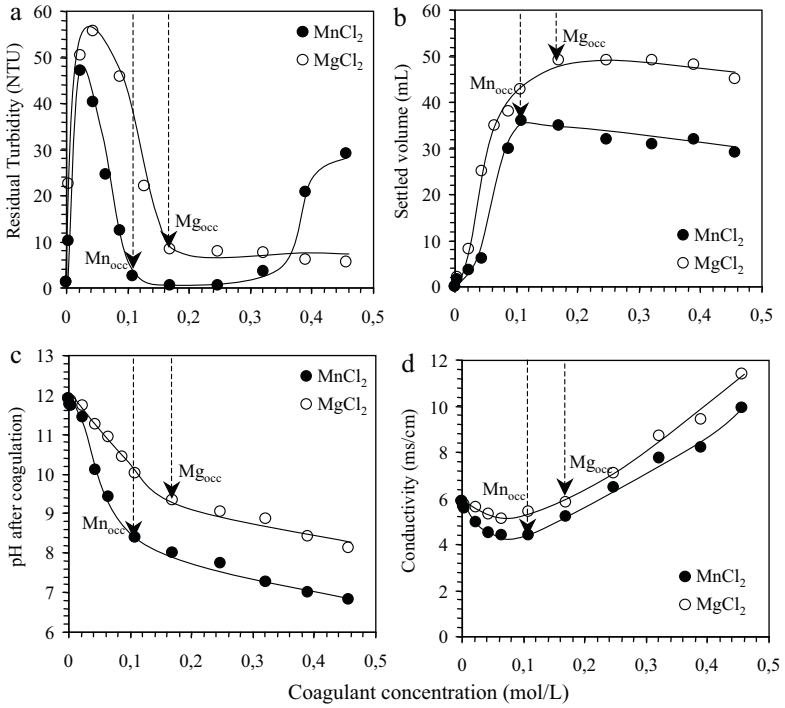

Fig. 1. Comparison of $MnCl_2$ (●) and $MgCl_2$ (○) coagulation performances for SW1: (a) residual turbidity, (b) sediment volume, (c) pH after coagulation, and (d) conductivity after coagulation. The arrows indicate the optimal coagulant concentrations.

persive X-ray spectrometry. The freeze-dried sediment was first re-suspended in ethanol under ultrasonication, and a drop of suspension was then evaporated on a carbon-coated copper grid. Elemental analysis was carried out with a 20 nm probe size, Kα X-ray emission lines of Na, S, Cl, Mg, Mn, being integrated and quantified after a 30 s counting time. Infrared analysis was conducted with a Bruker IFS 55 spectrophotometer in the transmission mode. 1 mg of freeze-dried sediment was mixed with 250 mg KBr (FTIR grade, Merck), and a pellet was prepared using a press connected to a vacuum pump. The spectra were recorded in the 4000–400 cm^{-1} range with 200 scans collected at 2 cm^{-1} resolution.

2.6. Adsorption isotherms

The adsorption experiments were performed using the precipitate obtained from the treatment of SW1 without EBRA dye at optimal coagulant concentration. Various amounts of the pigment dye were then added under slow mixing for 30 min, and the amount of adsorbed EBRA dye was calculated from the difference between the total added concentration and the supernatant concentration after 2 h settling.

3. Results and discussion

3.1. Jar test results

Figs. 1 and 2 compare the performance of $MnCl_2$ and $MgCl_2$ solutions in terms of turbidity removal, sediment volume, final pH, and conductivity after coagulation, for the two synthetic effluents SW1 and SW2. Similar patterns are observed for both coagulants: thus, residual turbidities (Figs. 1a and 2a) increase at low coagulant concentration to reach a maximum, and then decrease with further coagulant addition. The optimum coagulant concentrations (OCC) are defined as the minimum dosages to attain the low residual turbidity values (arrows in Figs. 1a and 2a). The OCC values found with a $MnCl_2$ treatment are slightly lower than those obtained with a $MgCl_2$ application, whereas the required coagulant demands for treating SW2 are almost double than those determined for SW1. This suggests that the negatively charged molecules of dyeing auxiliaries compete with the reactive dye for the coagulant species. Furthermore, the residual turbidity at OCC is lower for the manganese coagulant in the case of SW1, whereas in presence of all dyeing auxiliary chemicals (SW2), an equivalent turbidity removal is observed for both chemicals. Above OCC, the residual turbidities characterizing SW1 treatment are stable, and then strongly increased in the case of $MnCl_2$ coagulation. For turbidity curves obtained with SW2, the range of optimal dosing is reduced, as the residual turbidities slightly increase at higher coagulant concentrations.

All the sediments build-up from the lowest coagulant concentrations to reach a plateau around OCC (Figs. 1b and 2b). It is worth noting that $MnCl_2$ is clearly more effective than $MgCl_2$ in terms of sludge production, sediment volumes at OCC being 25–30% lower in the first case. Furthermore, the presence of dyeing auxiliary chemicals does not significantly increase the sediment volume generated by coagulation. The pH measurements show a marked decrease until OCC to reach a pH of about 9.4 and 8.3 for $MgCl_2$ and $MnCl_2$, respectively. Above OCC, the pH diminishes with a lesser slope in all cases. On the other hand, the conductivity slightly decreases at underdosages, and then increases proportionally with coagulant concentration above OCC. The color removal is illustrated in Fig. 3 as abatement rate vs coagulant concentration. For both SW1 and SW2, the percentage of EBRA dye removal strongly increases at low coagulant concentration and reaches about 90% at OCC. A complete removal can even be observed at slight overdosages.

3.2. Fate of dye and nature of coagulating species

At first approximation, the variations in turbidity, settled volume, pH, and conductivity, may simply be related to coagulant hydrolysis: the formation of an hydroxide precipitate can increase both residual turbidity and sediment volume, the associated

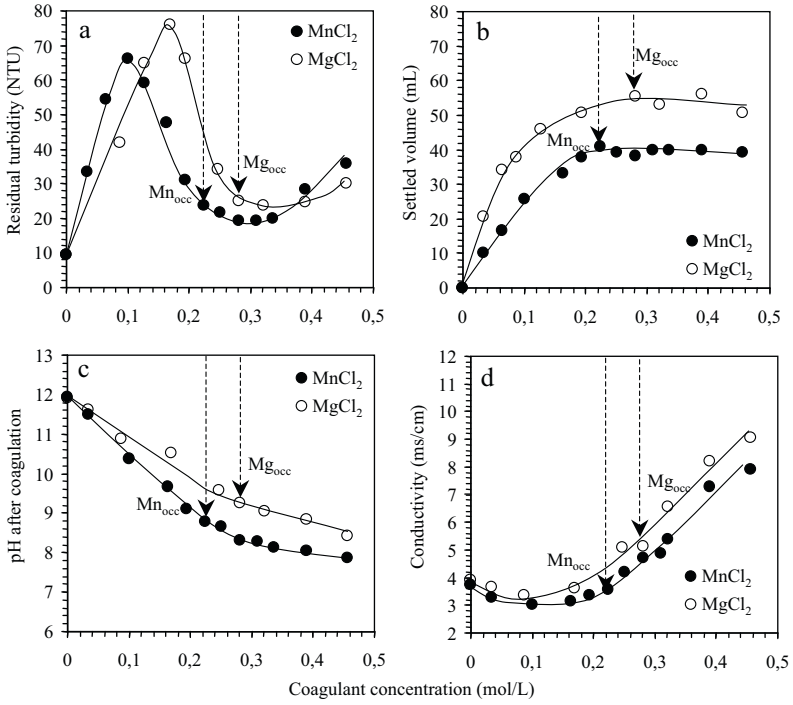

Fig. 2. Comparison of coagulation performances for SW2 (SW1 + dyeing auxiliaries): (a) residual turbidity, (b) sediment volume, (c) pH after coagulation, and (d) conductivity after coagulation. The arrows indicate the optimal coagulant concentrations.

OH^- consumption implying a drop in pH, and the corresponding decrease in conductivity being, in our case, likely compensated by the release of chloride ions from the added coagulants. Examination of hydroxide precipitates by TEM–EDXS shows that, during SW1 coagulation, both well-crystallized though irregular shaped platelets and small pseudo-cubic units are obtained with $MnCl_2$ (Fig. 4a), whereas monodispersed, but more poorly crystallized particles are formed with $MgCl_2$ (Fig. 4c). In contrast, nearly amorphous phases are precipitated during SW2 coagulation with either $MnCl_2$ or $MgCl_2$ (Fig. 4b and d), the crushed sheet texture of coagulating species being nevertheless reminiscent of previous plate-like particles.

EDXS microanalyses yield an atomic ratio Mg/O close to 0.5 for particles obtained with the $MgCl_2$ coagulant, which likely identifies a $Mg(OH)_2$–brucite precipitate. In the case of SW2 sediments, Mg/O is sometimes lower than 0.5 because of the oxygen content of the auxiliary dyeing chemicals associated with the precipitate. A slightly higher Mn/O of 0.6 characterizes the particles formed by hydrolysis of $MnCl_2$. Elemental analyses also indicate that minor amounts of sulfur, originating either from Subitol or Meropan, are associated with the hydroxide precipitate generated during SW2 coagulation. The electron diffraction patterns (insets Fig. 4c and d) confirm the presence of brucite in both SW1 and SW2 sediments (spacings at 2.39, 4.72, 1.82, 1.55 Å), but additional spacings at 3.05 and 2.04 Å suggest that part of original brucite has been converted to MgO–periclase under the electron beam [32]. Similarly, electron diffractograms of Mn-precipitates (insets Fig. 4a and b) reveal the presence in SW1 of feitknechite β-MnOOH (spacings at 4.62 and 2.64 Å), MnO_2–ramsdellite (weaker reflections at 4.04, 2.54 and 1.9 Å) that certainly results from electron beam damage to feitknechite, and hausmannite Mn_3O_4 (peak at 3.09 Å). The latter mineral may account for the Mn/O mean atomic ratio of 0.6 measured by EDXS. The precipitation of a mixture of feitknechite and hausmannite is actually expected when divalent manganese is hydrolyzed at basic pH under aerated conditions [33].

The infrared spectra taken from freeze-dried sediments allow to verify the presence of both brucite and hydrous manganese oxide (Fig. 5a). Brucite is characterized by a very sharp and intense peak at 3698 cm^{-1} (OH stretching vibration), a broad shoulder around 3212 cm^{-1} (strongly bonded water), and bands in the low frequency region at 638, 568, and 436 cm^{-1} (MgO translation modes) [34]. On the other hand, the absorption bands around 629, 525 and

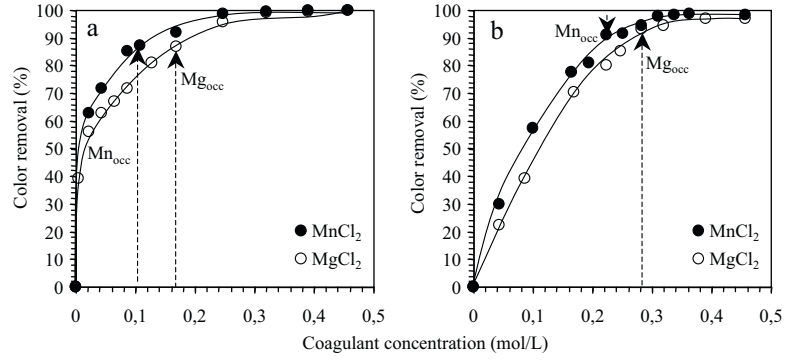

Fig. 3. Percentage of color removal as a function of coagulant concentration. (●) $MnCl_2$ and (○) $MgCl_2$. The arrows indicate the optimal coagulant concentrations.

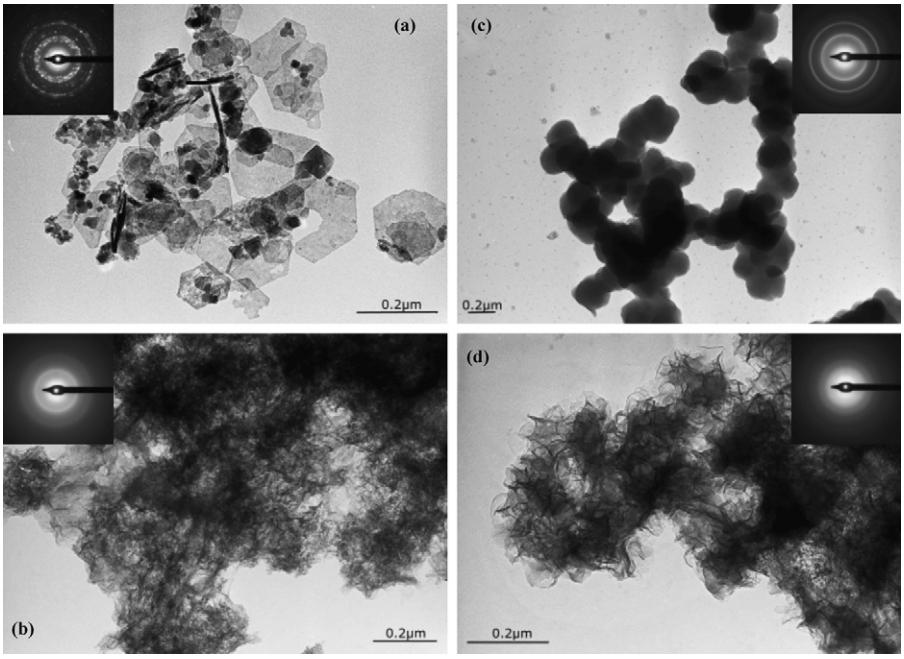

Fig. 4. Electron micrographs and electron diffraction patterns of freeze-dried coagulated sediments: (a) SW1 at $MnCl_2$ optimal concentration; well-crystallized platelets correspond to feitknechite whereas small pseudo-cubic minerals identify hausmannite. (b) SW2 at $MnCl_2$ optimal concentration. (c) SW1 at $MgCl_2$ optimal concentration. (d) SW2 at $MgCl_2$ optimal concentration.

418 cm^{-1} may be assigned to stretching vibrations of Mn–O bonds [35,36]. The bands of inorganic species largely dominate all spectra, even though EBRA dye (e.g. bands at 2924 and 2854 cm^{-1}) can be recognized in SW1 sediments, and urea and Migrasol (see Table 2 for peaks assignment) can be readily distinguished in SW2 sediments. It should be noted that part of EBRA dye molecules and auxiliary dyeing chemicals may have been removed during dialysis. The infrared spectra of various dyeing auxiliaries are presented in Fig. 5b. Peak positions and assignments are listed in Table 2. Closer examination of EBRA dye infrared features provides supplemen-

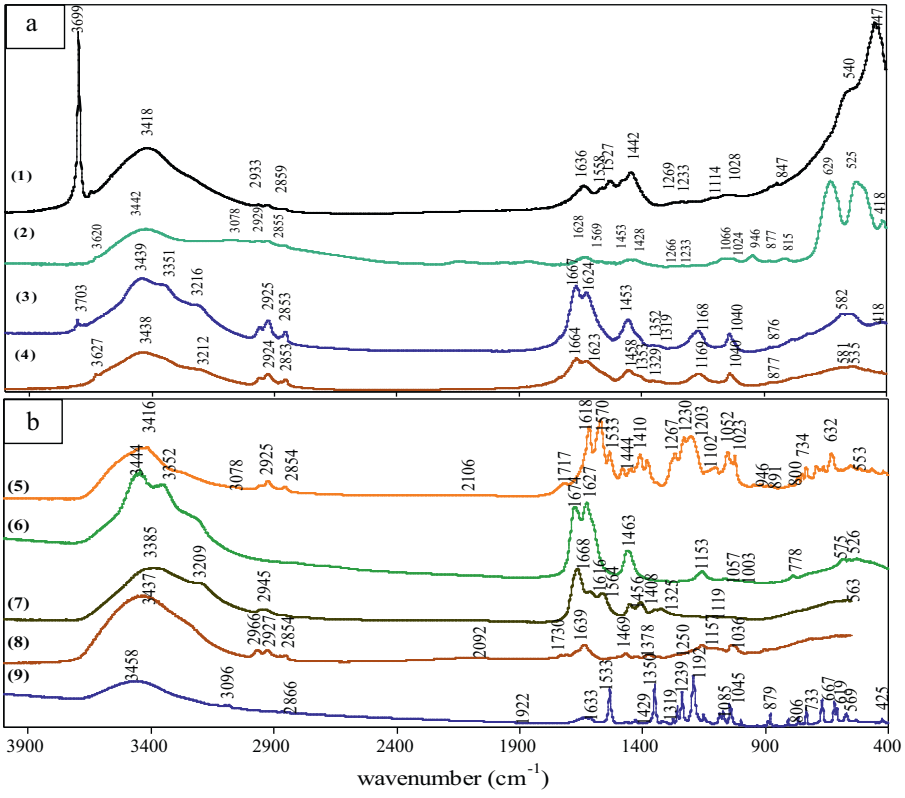

Fig. 5. (a) FTIR spectra of dialyzed and freeze-dried coagulated sediments: (1) SW1 at $MgCl_2$ optimal concentration; (2) SW1 at $MnCl_2$ optimal concentration; (3) SW2 at $MgCl_2$ optimal concentration; (4) SW2 at $MnCl_2$ optimal concentration. (b) FTIR spectra of EBRA dye and dyeing auxiliary chemicals: (5) EBRA dye; (6) urea; (7) Migrasol; (8) Subitol; (9) Rapidoprint. The peak assignments are given in Table 2.

Table 2
Main infrared absorption bands of EBRA dye pigment and dyeing auxiliaries. Peaks are assigned according to [42–44].

Band (cm^{-1})	Peak assignment
Urea	
1158	C–N stretching
1463	N–H deformation
1627	NH_2 deformation
1674	C=O stretching
Subitol	
903	S–O stretching
1000–1100	SO_3 symmetrical stretching
1100–1250	SO_3 asymmetrical stretching
1378	CH_3 deformation
1469	CH_2 deformation
1639	O–H deformation
Migrasol	
1177	C–N stretching
1349	C–H deformation
1408	N–H deformation
1456	CH_2 deformation
1564	NH_2 deformation
1616	C=C stretching
1668	C=O stretching
Rapidoprint	
1000–1100	SO_3 symmetrical stretching
1100–1250	SO_3 asymmetrical stretching
1350–1550	Ar–NO_2
800–1650	Ø meta substituted
EBRA dye	
157, 1444, 1410	Triazine
1000–1100	Aromatic rings stretching
1100–1200	Ar–F
1300–1400	NH–Ar
1400–1650	Aromatic rings deformation

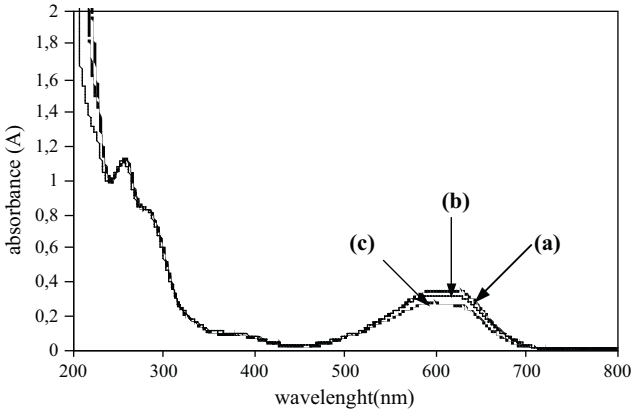

Fig. 6. UV–vis spectra of (a) EBRA dye solution acidified at pH 7; (b) SW1 coagulated with a slight overdose in $MgCl_2$ and then redissolved by acidification at pH 7; (c) SW1 coagulated with a slight overdose in $MnCl_2$ and then redissolved by acidification at pH 7.

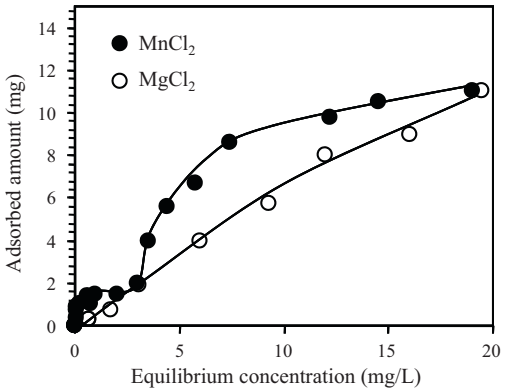

Fig. 7. Adsorption isotherms of EBRA dye onto hydrous manganese oxide at pH 8.3 (●) and brucite at pH 9.4 (○).

tary information on the molecule structure. Indeed, peaks at 1560, 1504, 1449 and 1410 cm^{-1} can be assigned to a triazine structure, the remaining bands corresponding to a substitution of aromatic rings.

No obvious interaction between the hydroxide precipitates and the EBRA dye pigment or the dyeing auxiliary chemicals could be evidenced using infrared spectroscopy. Actually, neither $Mg(OH)_2$ nor manganese hydrous oxide precipitation should alter the nature of EBRA dye. In the case of $MgCl_2$ addition, the sludge obtained remains bright blue, whereas the sediments generated by the $MnCl_2$ treatment process of SW1 and SW2 turn greenish because of the presence of strongly colored manganese minerals. Indeed, as illustrated in Fig. 6, almost identical UV–vis spectra are obtained from both initial SW1 solution at pH 7 and sediments coagulated with a slight overdose in $MgCl_2$ or $MnCl_2$ (0.32 mol/l) and then redissolved by acidification at neutral pH. The slight change in absorption around 600 nm is attributed to a small difference in dye concentration between the original and the redispersed sediments that results from the acidification.

3.3. Characteristics of the precipitation/adsorption mechanism

Eventually, though the treatment with $MgCl_2$ and $MnCl_2$ chemicals has been attributed hitherto to a coagulation with hydrolyzed species, the actual dye removal mechanism might better be described as a sorption phenomenon onto newly precipitated particles. The adsorption isotherms of EBRA molecules onto hydrous manganese oxide and magnesium hydroxide precipitates obtained from the respective optimal coagulant concentrations, are shown in Fig. 7. For magnesium hydroxide surfaces, the adsorbed amount of EBRA dye pigment increases steadily with the equilibrium concentration, whereas it shows two well-defined steps for hydrous manganese oxide particles thus confirming the dual nature of that precipitate. In addition, at any given equilibrium concentration, a larger adsorbed amount of EBRA dye pigment is consistently observed on manganese-based sorbents, which can be then related with the better removal efficiency obtained with the $MnCl_2$ treatment.

Such a precipitation/adsorption mechanism was initially proposed by Leentvaar and Rebhun [30] when investigating the action of $MgCl_2$ on domestic sewage. However, both EBRA molecule and dyeing auxiliary chemicals necessarily interfere with the hydrolyzing processes of $MgCl_2$ and $MnCl_2$. Indeed, the TEM micrographs and the electron diffraction patterns reveal a drastic change in the appearance and the cristallinity of precipitates generated during the treatment of SW1 and SW2 effluents. This can be attributed to an inhibition of hydroxide precipitate growth in the presence of EBRA molecule and/or dyeing auxiliaries. The latter effect can be readily evidenced by comparing EBRA dye removal onto already precipitated $Mg(OH)_2$ or MnOOH particles at various $MgCl_2$ or $MnCl_2$ concentrations, with the original jar-tests carried out with SW1 solutions. As shown in Fig. 8, both the turbidity and the color removal curves are shifted towards higher coagulant concentrations when the dye is added after the formation of precipitates, thus implying a poorer elimination of the contaminant. The higher removal efficiency observed during jar-tests can be explained by the adsorption of EBRA dye pigment to the active growth sites of the precipitate, thus limiting the size of particles formed, and hence increasing both its specific surface area and its adsorption capacity. In the case of SW2 effluents, the presence of a larger

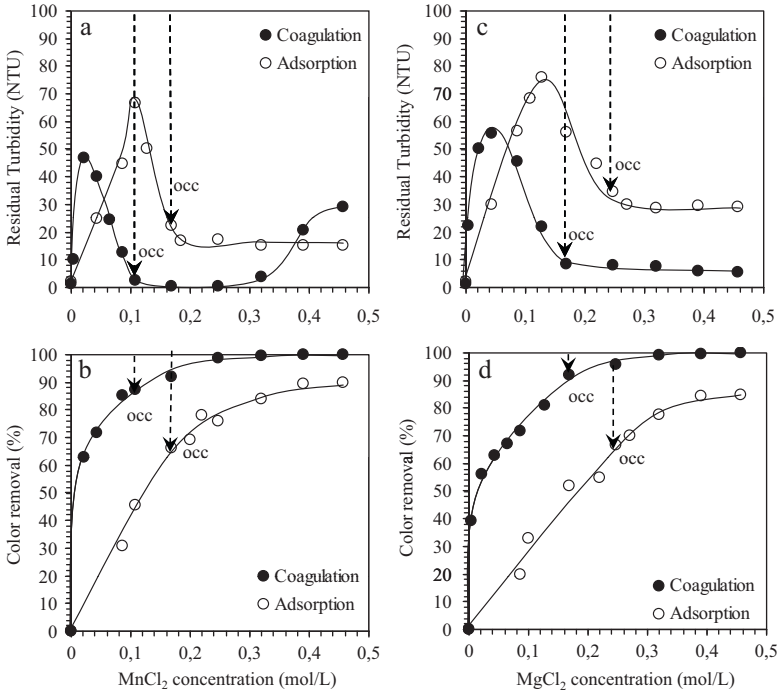

Fig. 8. Comparison of EBRA dye removal by coagulation (●) and adsorption onto brucite or hydrous manganese oxide precipitated at various concentrations (○). (a) Residual turbidity vs $MnCl_2$ concentration; (b) color removal vs $MnCl_2$ concentration; (c) residual turbidity vs $MgCl_2$ concentration; (d) color removal vs $MgCl_2$ concentration.

amount of additives further inhibits the formation of particles (Fig. 4b–d).

3.4. Behavior of aggregated suspensions under agitation

In accordance with the precipitation/adsorption mechanism suggested above, the pHs reached at the optimal coagulant concentration are (i) close to the pH of $Mg(OH)_2$ formation in high alkalinity solutions [37] and (ii) similar to the point of zero charge (8.3) determined for hydrous manganese oxide in the case of $MnCl_2$ treatment [38]. Therefore, the surfaces of precipitated particles should carry no net charge at the optimal treatment concentration, and the aggregates thus obtained should behave according to a charge neutralisation mechanism [45]. Fig. 9 shows the variation in mean aggregate size under cyclic step changes in agitation intensity, for SW1 and SW2 treated with optimal concentrations of $MnCl_2$ and $MgCl_2$, respectively. In all cases, the size of aggregates slowly decreases at the initial constant stirrer speed of 100 rpm. As those aggregates were prepared from the coagulated suspensions redispersed in their respective synthetic solutions, the observed decrase in aggregate size can certainly be attributed to that dilution stage provided that a dynamic exchange between the aggregated material does exist [31]. Upon an increase in stirring (300 rpm), the flocs break up first rapidly and then more slowly. When the agitator speed is reset to its initial value (100 rpm), the aggregate reform rapidly but to a size about half smaller than that obtained just

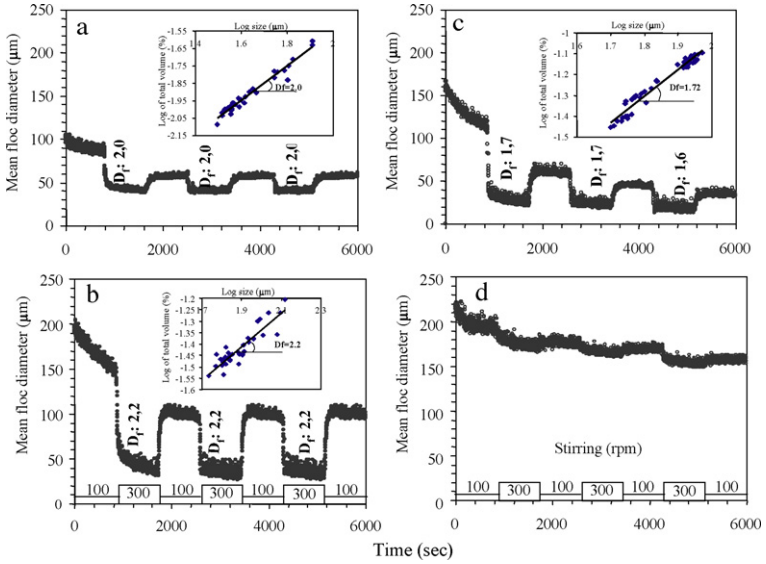

Fig. 9. Evolution of average floc size as a function of time under consecutive cyclic step changes in agitation intensity. The insets show examples of the determination of the floc mass fractal dimension. (a) SW1 treated with $MnCl_2$; (b) SW2 treated with $MnCl_2$; (c) SW1 treated with $MgCl_2$; (d) SW2 treated with $MgCl_2$.

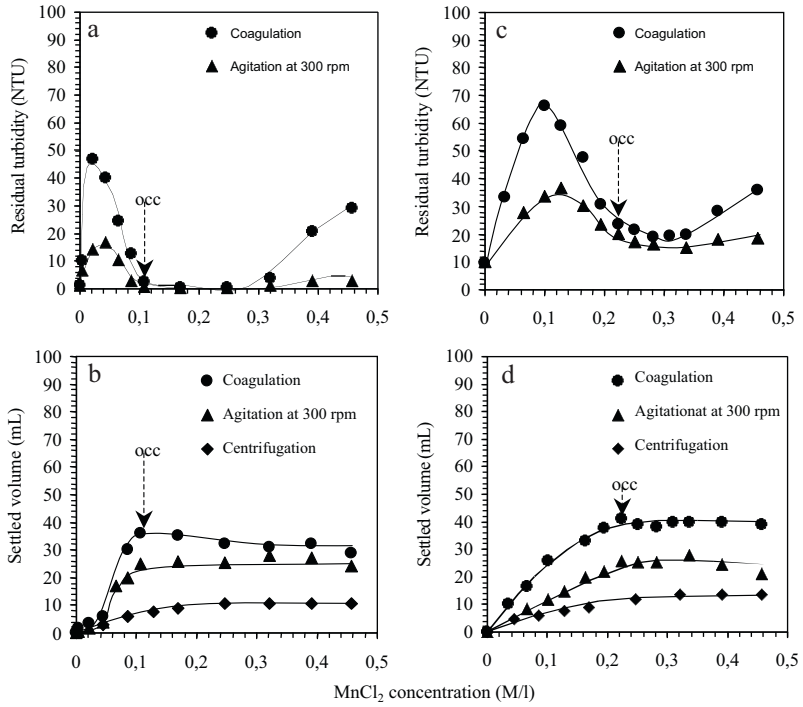

Fig. 10. Effect of further agitation at 300 rpm and centrifugation at 2860 × *g* on residual turbidity and sediment volume. (a and b) SW1 treated with $MnCl_2$; (c and d) SW2 treated with $MnCl_2$.

before initiating the first increase in shearing. Further cycling of agitation conditions between high and low levels of intensity, reveals that floc break-up and floc re-aggregation become nearly reversible for aggregates generated with a $MnCl_2$ treatment. Such behavior is consistent with a charge-neutralisation destabilisation mechanism [31]. In contrast, the aggregates obtained after a $MgCl_2$ application only partially reforms after shearing. This may be attributed to the nature of brucite precipitate which, as illustrated in Fig. 4c, looks like intergrown agglomerates that may not rebuild once broken.

The insets of Fig. 9 show typical log–log plots of aggregate volume fraction vs mean floc size obtained during the consecutive cyclic step changes in stirring. Obviously, the range of mean floc size determined here limits the applicability of the power–law relationship to barely one decade in length, which cannot be considered sufficient to define a true fractal dimension. In the particular case of the synthetic effluent SW2 treated with the $MgCl_2$ solution, such

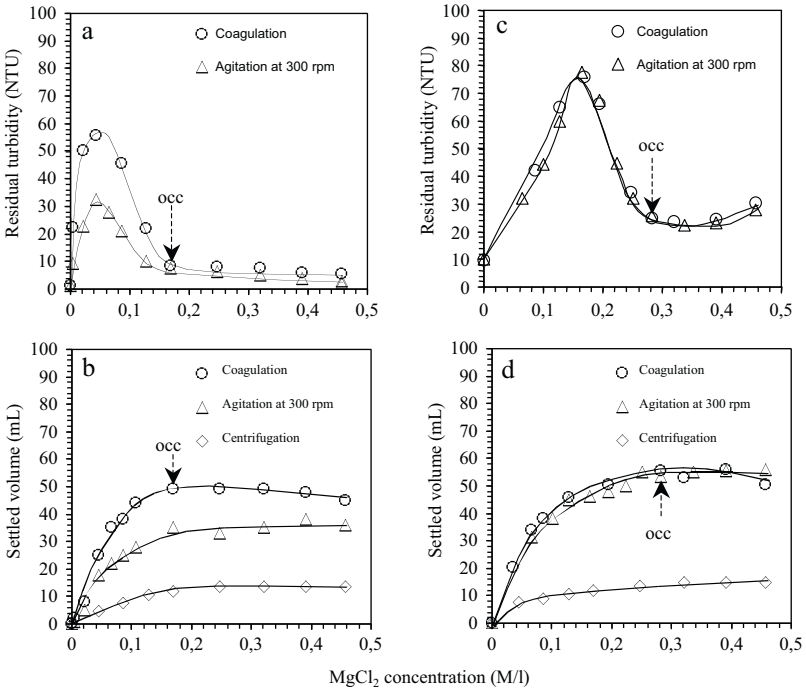

Fig. 11. Effect of further agitation at 300 rpm and centrifugation at 2860 × *g* on residual turbidity and sediment volume. (a and b) SW1 treated with $MgCl_2$; (c and d) SW2 treated with $MgCl_2$.

exponent cannot even be determined (Fig. 9d). Nevertheless, the D_f values thus obtained are consistent with classical aggregation mechanisms reported in the literature. Thus, the D_f value close to 1.7 calculated for aggregates resulting from the application of $MgCl_2$ to the SW1 effluent, may be ascribed to a diffusion-limited cluster aggregation mechanism [39]. Likewise, the scaling exponent slightly above 2 found with $MnCl_2$ treatments (Fig. 9a and b) could be attributed a reaction-limited aggregation. However, in the latter case, the aspect ratio of the hydrous MnOOH particles likely influences the arrangement of elementary particles within the aggregates.

At first approximation, the constant D_f values during the cyclic changes in stirring suggest that no major aggregate restructuring has occurred. However, as shown in Figs. 10 and 11, both residual turbidity and sediment volume decreased significantly after increased agitation at 300 rpm except in the case of SW2 effluent treated with $MgCl_2$ (Fig. 11c and d). A rearrangement of aggregates to more compact fractal structures when the flocs are exposed to increased shear has already been demonstrated in the literature [40]. In our case, such restructuring certainly occurs at a smaller length scale than that investigated by the laser sizer. Figs. 10 and 11 suggest that such phenomenon can be exploited to decrease the amount of sediment generated by the application of $MnCl_2$ or $MgCl_2$. Indeed, simple centrifugation at $2860 \times g$ allows to further diminish the sludge volume after treatment.

4. Concluding remarks

The results presented in this paper shed new light on the mechanisms involved when either $MnCl_2$ or $MgCl_2$ solutions are used for removing dye pigment from textile effluents. In both cases, the removal mechanism can be attributed to the adsorption of the dye pigment onto the forming hydroxyde precipitate. Most dyeing auxiliary chemicals compete with the reactive dye for the precipitated particles, and hence significantly increase the required coagulant demand for optimal dye elimination.

Previous literature has shown that the use of $MgCl_2$ is economically viable [23], especially since magnesium can be easily recovered and reused [29]. In textile manufacturing plants close to the sea, further cost reduction can certainly be achieved if sea water is used as a source of magnesium ion. The application of $MnCl_2$ for the treatment of textile dye wastes appears to represent a promising alternative approach since both optimal dosage and sludge production are significantly lower than those achieved with $MgCl_2$. The residual manganese concentrations measured by atomic absorption spectroscopy are less than 0.01 ppm and 0.37 ppm for the treatment of SW1 and SW2, respectively. Such values comply with the environmental standards on liquid effluent disposal in surface waters. The application of $MnCl_2$ to textile wastes can also certainly be optimized to preferentially yield the hydrous manganese oxide mineral that is the most efficient for color removal.

Acknowledgement

A.Z.B. and S.K. would like to thank the Ministry of Higher Education and Scientific Research of Algeria for financial support.

References

[1] I. Petrinić, P.R.A. Andersen, S. Šostar-Turk, A.M. Le Marechal, The removal of reactive dye printing compounds using nanofiltration, Dyes Pigments 74 (3) (2007) 512–518.
[2] M.M. Karim, A.K. Das, S.H. Lee, Treatment of colored effluent of the textile industry in Bangladesh using zinc chloride treated indigenous activated carbons, Anal. Chim. Acta 576 (1) (2006) 37–42.
[3] D.J. Joo, W.S. Shin, J.H. Choi, S.J. Choi, M.C. Kim, M.H. Han, T.W. Ha, Y.H. Kim, Decolorization of reactive dyes using inorganic coagulants and synthetic polymer, Dyes Pigments 73 (1) (2007) 59–64.
[4] I. Koyuncu, Influence of dyes salts and auxiliary chemicals on the nanofiltration of reactive dye baths: experimental observations and model verification, Desalination 154 (1) (2003) 79–88.
[5] A.L. Ahmad, S.W. Puasa, Reactive dyes decolourization from an aqueous solution by combined coagulation/micellar-enhanced ultrafiltration process, Chem. Eng. J. 132 (1-3) (2007) 257–265.
[6] S. Papic, N. Koprivanac, A.L. Bozic, A. Metes, Removal of some reactive dyes from synthetic wastewater by combined Al(III) coagulation/carbon adsorption process, Dyes Pigments 62 (2004) 291–298.
[7] A.B. Dos Santos, F.C.J. Cervantes, J.B. van Lier, Review paper on current technologies for decolourisation of textile wastewaters: perspectives for anaerobic biotechnology, Bioresour. Technol. 98 (12) (2007) 2369–2385.
[8] A. Uygur, E. Kok, Decolorisation treatments of azo dye wastewaters including dichlorotriazinyl reactive groups by using advanced oxidation method, J. Soc. Dyers Colour 115 (1999) 350–354.
[9] I. Arslan, I.A. Balcioglu, Degradation of commercial reactive dyestuffs by heterogenous and homogenous advanced oxidation processes: a comparative study, Dyes Pigments 43 (1999) 95–108.
[10] M. Muruganandham, M. Swaminathan, Photochemical oxidation of reactive azo dye with UV–H_2O_2 process, Dyes Pigments 62 (2004) 269–275.
[11] A.G. Vlyssides, M. Loizidou, P.K. Karlis, A.A. Zorpas, D. Papaioannou, Electrochemical oxidation of a textile dye wastewater using a Pt/Ti electrode, J. Hazard. Mater. 70 (1999) 41–52.
[12] B.K. Körbahti, A. Tanyolac, Electrochemical treatment of simulated textile wastewater with industrial components and Levafix Blue CA reactive dye: optimization through response surface methodology, J. Hazard. Mater. 151 (2–3) (2007) 422–431.
[13] D. Rajkumar, B.J. Song, J.G. Kim, Electrochemical degradation of Reactive Blue 19 in chloride medium for the treatment of textile dyeing wastewater with identification of intermediate compounds, Dyes Pigments 72 (1) (2007) 1–7.
[14] G. Sudarjanto, B. Keller-Lehmann, J. Keller, Optimization of integrated chemical–biological degradation of a reactive azo dye using response surface methodology, J. Hazard. Mater. 138 (2006) 160–168.
[15] C. O'Neill, F.R. Hawkes, D.L. Hawkes, S. Esteves, S.J. Wilcox, Anaerobic–aerobic biotreatment of simulated textile effluent containing varied ratios of starch azo dye, Water Res. 34 (2000) 2355–2361.
[16] Y.R. Yu-Li, A. Thomas, Color difference measurement and color removal from dye wastewaters using different adsorbents, J. Chem. Technol. Biotechnol. 63 (1995) 55–59.
[17] A. Bousher, X. Shen, R.G.J. Edyvean, Removal of coloured organic matter by adsorption onto low-cost waste materials, Water Res. 31 (1997) 2084–2092.
[18] R. Dolphen, N. Sakkayawong, P. Thiravetyan, W. Nakbanpote, Adsorption of Reactive Red 141 from wastewater onto modified chitin, J. Hazard. Mater. 145 (1–2) (2007) 250–255.
[19] S. Papic, N. Koprivanac, A. Loncaric Bozic, Removal of reactive dyes from wastewater using Fe(III) coagulant, J. Soc. Dyers Colour 116 (2000) 352–358.
[20] B. Shi, G. Li, D. Wang, C. Feng, H. Tang, Removal of direct dyes by coagulation: the performance of preformed polymeric aluminum species, J. Hazard. Mater. 143 (1–2) (2007) 567–574.
[21] B.Y. Gao, Q.Y. Yue, Y. Wang, W.Z. Zhou, Color removal from dye-containing wastewater by magnesium chloride, J. Environ. Manage. 82 (2) (2007) 167–172.
[22] V. Golob, A. Vinder, M. Simonič, Efficiency of the coagulation/flocculation method for the treatment of dyebath effluents, Dyes Pigments 67 (2) (2005) 93–97.
[23] B.H. Tan, T.T. Teng, A.K. Mohd Omar, Removal of dyes and industrial dye wastes by magnesium chloride, Water Res. 34 (2) (2000) 597–601.
[24] C. Allègre, M. Maisseu, F. Charbit, P. Moulin, Coagulation–flocculation–decantation of dye house effluents: concentrated effluents, J. Hazard. Mater. 116 (2004) 57–64.
[25] J.W. Lee, S.P. Choi, R. Thiruvenkatachari, W.G. Shim, H. Moon, Evaluation of the performance of adsorption and coagulation processes for the maximum removal of reactive dyes, Dyes Pigments 69 (3) (2006) 196–203.
[26] N. Al-Bastaki, Removal of methyl orange dye and Na_2SO_4 salt from synthetic waste water using reverse osmosis, Chem. Eng. Process. 43 (12) (2004) 1561–1567.
[27] J. Porter, A.C. Gomes, The rejection of anionic dyes and salt from water solutions using a polypropylene microfilter, Desalination 128 (2000) 81–90.
[28] C. Allègre, P. Moulin, M. Maisseu, F. Charbit, Treatment and reuse of reactive dyeing effluents, J. Membr. Sci. 269 (1–2) (2006) 15–34.
[29] J.F. Judkins, J.S. Hornsby, Color removal from textile dye waste using magnesium carbonate, J. Water Pollut. Control Fed. 50 (11) (1978) 2446–2456.
[30] J. Leentvaar, M. Rebhun, Effect of magnesium and calcium precipitation on coagulation–flocculation with lime, Water Res. 16 (1982) 655–662.
[31] V. Chaignon, B.S. Lartiges, A. El Samrani, C. Mustin, Evolution of size distribution and transfer of mineral particles between flocs in activated sludges: an insight into floc exchange dynamics, Water Res. 36 (2002) 676–684.
[32] J.A. Wang, O. Novaro, X. Bokhimi, T. Lopez, R. Gomez, J. Navarette, M.E. Llanos, E. Lopez-Salinas, Characterizations of the thermal decomposition of brucite prepared by sol–gel technique for synthesis of nanocrystalline MgO, Mater. Lett. 35 (1998) 317–323.
[33] J.D. Hem, C.J. Lind, Nonequilibrium models for predicting forms of precipitated manganese oxides, Geochim. Cosmochim. Acta 47 (1983) 2037–2046.

[34] R.L. Frost, J.T. Kloprogge, Infrared emission spectroscopic of brucite, Spectrochim. Acta, Part A 55 (1999) 2195–2205.
[35] T. Kohler, T. Armbruster, E. Libowitzky, Hydrogen bonding and Jahn–Teller distortion in Groutite α-MnOOH and Manganite γ-MnOOH, and their relations to the manganese dioxides Ramsdellite and Pyrolusite, J. Solid State Chem. 133 (1997) 486–500.
[36] C.M. Julien, M. Massot, C. Poinsignon, Lattice vibrations of manganese oxides Part I. Periodic structures, Spectrochim. Acta, Part A 60 (2004) 689–700.
[37] E.L. Berg, C.A. Brummer, W.T. Williams, Single stage lime clarification, Water Waste Eng. 7 (1970) 3–42.
[38] M. Ramstedt, B.M. Andersson, A. Shchukarev, S. Sjöberg, Surface properties of hydrous manganite (γ-MnOOH). A potentiometric, electroacoustic, and X-ray photoelectron spectroscopy study, Langmuir 20 (2004) 8224–8229.
[39] P Meakin, Fractal aggregates, Adv. Colloid Interface Sci. 28 (1998) 249–331.
[40] P.T. Spicer, S.E. Pratsinis, J. Raper, R. Amal, G. Bushell, G. Meesters, Effect of shear schedule on particle size, density, and structure during flocculation in stirred tanks, Powder Technol. 97 (1998) 26–34.
[41] A.Z. Bouyakoub, S. Kacha, B.S. Lartiges, S. Bellebia, Z. Derriche, Treatment of reactive dye solutions by physicochemical combined process, Desalinat. Water Treat. 12 (1–3) (2009) 202–209.
[42] C.J. Pouchert, The Aldrich Library of FTIR Spectra, 1st ed., Aldrich Chemical Company, Inc., 1985.
[43] N.B. Colthup, L.H. Daly, S.E. Wibertey, Introduction to Infrared and Raman Spectroscopy, 2nd ed., Academic Press, 1975, pp. 376–381.
[44] C.N.R. Rao, Chemical Application of Infrared Spectroscopy, Academic Press, Inc., 1963, pp. 324–325.
[45] W. Stumm, J.J. Morgan, Aquatic Chemistry, Chemical Equilibria and Rates in Natural Waters, 3rd ed., John Wiley & Sons, Inc., New York, 1996, pp. 349–424.